

Article

Synthesis of Up-Conversion Fluorescence N-Doped Carbon Dots with High Selectivity and Sensitivity for Detection of Cu²⁺ Ions

Yuanyuan Xiong, Mengxiao Chen, Zhen Mao, Yiqing Deng, Jing He, Huaixuan Mu, Peini Li, Wangcai Zou and Qiang Zhao * 

School of Chemical Engineering, Sichuan University, No. 24 South Section 1, Yihuan Road, Chengdu 610065, China; xiongyuanyuan@stu.scu.edu.cn (Y.X.); cmx961012@163.com (M.C.); maozhenjqk@163.com (Z.M.); dengyiqing@stu.scu.edu.cn (Y.D.); hejing7@stu.scu.edu.cn (J.H.); mhx@stu.scu.edu.cn (H.M.); lipeini@stu.scu.edu.cn (P.L.); zouwangcai@stu.scu.edu.cn (W.Z.)

* Correspondence: zhaoqiang@scu.edu.cn

Abstract: Carbon dots have drawn extensive attention in the detection of metal ions with good stability, excellent biocompatibility and low toxicity. Meanwhile, the quantum yield, response rate and the detection mechanism for Cu²⁺ ions are vital to their development and application. To obtain more selective and sensitive materials to detect Cu²⁺ ions, N-doped carbon dots (DN-CDs) were synthesized by a one-step hydrothermal method using citric acid as the carbon source and diethylenetriamine (DETA) as the nitrogen source. The obtained DN-CDs exhibited stable and intense blue light emission and special near-infrared up-conversion fluorescence at 820 nm, attributed to the effect of introducing N atoms into the structure of carbon dots. Due to the dynamic quenching of the DN-CDs by Cu²⁺ ions, the fluorescence intensity ($\lambda_{\text{ex}} = 820 \text{ nm}$) of DN-CDs was quantitatively decreased in the presence of Cu²⁺ ions. The DN-CDs had a rapid response within 3 min. The DN-CD system exhibited a linear relationship with a concentration range from 2.5 to 50 μM and low detection limit (LOD) of 42 nM. After careful investigation, an interesting conclusion was proposed: N-doped CDs with N/O = 1:1 or higher with relatively abundant N atoms prefer to detect Cu²⁺ ions while those with N/O = 1:2 or lower prefer to detect Fe³⁺ ions.

Keywords: carbon dots; up-conversion fluorescence; Cu²⁺ ions detection



Citation: Xiong, Y.; Chen, M.; Mao, Z.; Deng, Y.; He, J.; Mu, H.; Li, P.; Zou, W.; Zhao, Q. Synthesis of Up-Conversion Fluorescence N-Doped Carbon Dots with High Selectivity and Sensitivity for Detection of Cu²⁺ Ions. *Crystals* **2023**, *13*, 812. <https://doi.org/10.3390/cryst13050812>

Academic Editor: Paolo Olivero

Received: 14 April 2023

Revised: 8 May 2023

Accepted: 10 May 2023

Published: 13 May 2023



Copyright: © 2023 by the authors. Licensee MDPI, Basel, Switzerland. This article is an open access article distributed under the terms and conditions of the Creative Commons Attribution (CC BY) license (<https://creativecommons.org/licenses/by/4.0/>).

1. Introduction

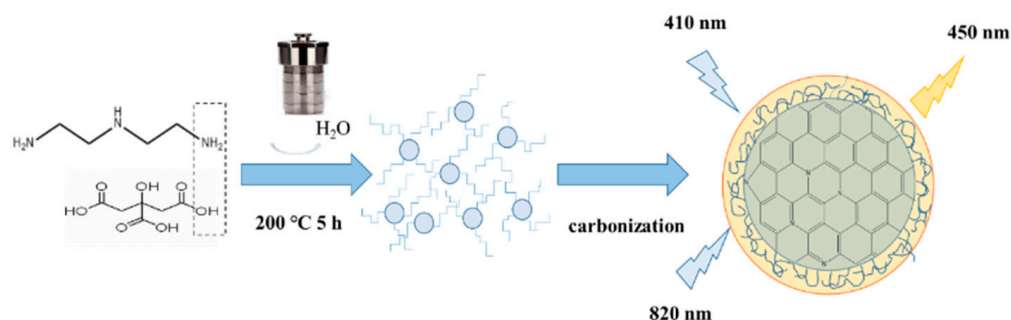
Industrial pollutants pose serious threats to nature and human health, so their removal and detection are extremely important. At present, some effective materials have been developed for the removal of pollutants, such as chitosan-based polymer materials with excellent adsorption abilities for heavy metal ions [1]. Additionally, some effective analytical methods have been developed to detect chemical or biological drugs, metal ions and organic pollutants [2–5]. Analytical methods used to detect metal ions include potential/electrochemical sensors [6,7], fluorescence analysis [8], atomic absorption spectrometry (AAS) [9] and inductively coupled plasma mass spectrometry (ICP-MS) [10]. However, most of these approaches are not suitable for real-time monitoring due to their high cost, long assay times, special equipment, and laborious and complex experimental processes. Therefore, fluorescent sensors with low cost, simple operation, high sensitivity and good selectivity have gradually emerged [11]. Nowadays, various materials have been developed as fluorescent probes for environmental monitoring of metal ions, such as metal–organic frameworks (MOFs) [12,13], nanoclusters [14,15], organic fluorescent dyes [16] and semiconductor quantum dots. In particular, fluorescent carbon-based materials have attracted extensive attention due to their good chemical stability, excellent biocompatibility and low toxicity [17], distinguishing themselves from traditional fluorescent materials.

With the progress in scientific and technological research, more heavy metals remain in the human living environment. The excessive intake of metal ions will have extremely serious effects on human health [18,19]. Copper is one of the most important transition metals in the human body [20] and plays an extremely important role in biological processes, such as embryonic development, mitochondrial respiration, regulation of hemoglobin levels as well as hepatocyte and neuronal functions [21,22]. Copper ions are widely distributed in the natural environment, especially in industrial wastewater. Long-time exposure to copper ions will cause high toxicity to the human body, and is associated with neurodegenerative diseases, such as Wilson's syndrome, Alzheimer's disease and Parkinson's disease [23–25]. According to United States Environmental Protection Agency (USEPA) guidelines, drinkable water must not contain a Cu^{2+} content of $\geq 20 \mu\text{M}$ [26]. Therefore, the detection of copper ions in the environment requires a simple and practical detection method with high sensitivity and selectivity.

Carbon dots (CDs) are zero-dimensional carbon-based materials, mostly spherical nanoclusters with diameters of less than 10 nm, composed of amorphous or crystalline cores with sp^2 hybrid carbon atoms [27]. Owing to their small size, high photostability, resistance to photobleaching, low toxicity, good water solubility, excellent biocompatibility and ease of surface functionalization, carbon dots have become the focus of fluorescent probe materials as well as in cell labeling, optical bioimaging, drug delivery, storage applications and photocatalysis [28]. Metal ions, such as Hg^{2+} , Fe^{3+} and Cu^{2+} , can effectively quench the fluorescence of carbon dots [29–31]. Carbon dots can be obtained by thermal decomposition [32], hydrothermal carbonization [33], microwave-assisted pyrolysis [34], electrochemical methods [35], etc. Hydrothermal carbonization refers to heating water and carbon-rich substances in a closed container to trigger the carbonization reaction. Citric acid is the most used carbon-rich substance, which is easy to condense and induce to form carbon rings, and is also has atoms that can be easily doped. Meanwhile, the surface of the formed carbon dots has rich functional groups, such as hydroxyl and carboxyl groups. The hydrothermal method is the most widely used method, which has the characteristics of good feasibility; cheap, diverse carbon sources; no toxicity; and environmental friendliness [36]. However, carbon dots without modification usually have a low quantum yield (QY) and poor stability, which affect their practical application [37,38]. Additionally, the origin of fluorescence in carbon dots has not yet been clarified. The fluorescence emission is primarily caused by the competition between the optical centers, surface states and traps [39]. Up-conversion fluorescence means that the shorter wavelengths of light are emitted through longer excitation wavelengths [40]. This fluorescence is usually caused by the multiphoton absorption effect. The fluorescence of carbon dots can be altered by controlling size and shape, modifying the edges of the surfaces and doping with heteroatoms, due to the edge effect, surface effect and quantum confinement effect (QCE) [41]. Doping different elements leads to better performance, such fluorescence improvement and shifting of the fluorescence spectra. Doping with different heteroatoms can change the electronic properties and excite special optical properties through the passivation of the surface states or the introduction of defects [42,43]. Salehtabar et al. [44] prepared photo-luminescent, water-soluble, nitrogen-doped, highly fluorescent carbon dots based on the gum tragacanth polysaccharide and triethylenetetramine (TETA). Therefore, it is a better way to synthesize fluorescent probe materials based on carbon dots with a higher sensitivity, higher selectivity, high quantum yield and unique fluorescence performance.

Herein, we report a simple method for preparing nitrogen-doped carbon dots (DN-CDs) with intense down-conversion and unique up-conversion fluorescence using diethylenetriamine (DETA) and citric acid as the nitrogen and carbon sources, respectively (Scheme 1). The DN-CDs had good fluorescence properties, and excellent photobleaching and stability. We used it for rapid, efficient and selective detection of copper ions within 3 min with a detection limit (LOD) as low as 42 nM. Compared with other carbon dots, DN-CDs showed better and stable up-conversion fluorescence, which could convert low energy light into high energy radiation through a nonlinear optical process, avoiding in-

interference with biological background luminescence and achieving good photon tissue penetration [45–48]. This would compensate for the disadvantages of down-conversion fluorescence carbon dots, and has great potential for detecting metals in organisms. The experimental results proved that the mechanism of fluorescence quenching through dynamic quenching. Additionally, combined with reports in the literature, the ratio of N and O atoms may be more critical on the premise that the N, O-based functional groups interact with Cu^{2+} . Two previously synthesized nitrogen-doped carbon dots were selected for comparison and preliminarily verified the proposed conclusion. This would be conducive to the selection and design of highly selective fluorescent probe materials for copper ions.



Scheme 1. Schematic illustration for DN-CD preparation.

2. Experimental

2.1. Chemicals and Materials

All chemicals were of analytical grade and were used directly without any further purification. Diethylenetriamine, quinine sulfate and all the metal nitrates, nicotinamide sulfate and chloride salts were purchased from Kelong Chemical Co., Ltd. (Chengdu, China). Citric acid and sulfuric acid were purchased from Xilong Chemical Co., Ltd. (Chengdu, China). Anhydrous ethanol was purchased from Changlian Chemical Co., Ltd. (Chengdu, China). N, N-Dimethylformamide (DMF) and Tetrabutylammonium Tetrafluoroborate were purchased from Dingsheng Chemical Co., Ltd. (Chengdu, China). l-Glutamic acid (l-Glu) and m-phenylenediamine (MPD) were purchased from Aladdin Industrial Co., Ltd. (Shanghai, China).

2.2. Preparation of N-CDs

N-doped carbon dots were synthesized by a simple one-step hydrothermal method. First, 0.44 g citric acid (CA) and a certain amount of diethylenetriamine (DETA) were added to 20 mL of ultra-pure water and sonicated for 20 min until the CA was dissolved. The prepared mixture was placed in a 50 mL PPL-lined stainless-steel autoclave and heated in an oven for a certain amount of time. The autoclave was cooled to room temperature after the reaction, and a slightly yellow solution was obtained. The solution was collected, dialyzed (MWCO = 500 Da) for 24 h to remove unreacted starting materials and then the dialysate was removed and internal solution was freeze-dried to obtain the final brown product. The optimal amount of DETA was determined by testing the varying molar ratios of CA:DETA (1:1, 1:2, 1:4, 1:8 and 1:10) with the reaction condition of 5 h and 180 °C. Additionally, the optimal reaction temperature was determined by testing different temperatures (150 °C, 180 °C, 200 °C, 220 °C and 240 °C) with a 1:4 molar ratio of CA:DETA and 5 h reaction time. Then, the reaction time was determined by testing different reaction times (4 h, 6 h, 8 h, 10 h and 12 h) with a 1:4 molar ratio of CA:DETA at 200 °C.

The two other carbon dots were prepared according to previous reports [49,50]. The specific preparation methods are detailed in the Supplementary Information.

2.3. Measurement of Quantum Yield

DN-CDs have similar absorption peaks (350 nm) and emission peaks (380–580 nm) as quinine acid; therefore, the QY could be measured using a relative method [51]. Quinine sulfate was selected as the reference compound (QY = 54% in 0.05 M H₂SO₄). The QY of our sample was calculated using Equation (1):

$$Y_1 = Y_2 \frac{S_1 A_2 n_1^2}{S_2 A_1 n_2^2} \quad (1)$$

where 'Y₁' is the QY of DN-CDs, 'Y₂' is the QY of quinine sulfate, 'S' is the peak area obtained from emission peak integration, 'A' is the absorbance intensity at λ(ex) of 350 nm, and 'n' is the refractive index (1.33 for both sample and reference). A series of solutions of DN-CDs and quinine sulfate were prepared until the absorbance intensities were below 0.05 at λ_{ex} = 350 nm, which were recorded as A₁ and A₂, respectively. Then, the fluorescence spectra were measured and the emission peaks in the range of 400–700 nm were selected for integration to obtain the peak areas (S₁ and S₂). Finally, the QY for our DN-CDs was calculated using Equation (1).

2.4. Characterization

Transmission electron microscopy (TEM) was performed using an INSPECT F instrument (J&R Instrument Technology Co., Ltd., Shanghai, China). X-ray photoelectron spectroscopy (XPS) results were obtained using XSAM 800 equipment (Kratos Analytical Ltd., Manchester, UK). The X-ray diffraction (XRD) patterns were identified using an X'Pert PRO diffractometer (PANalytical, Almelo, The Netherlands) with Cu Kα1 radiation, a step size of 0.01313° 2θ, and a counting time of 30 ms step⁻¹ from 10° to 80°. FT-IR spectra were obtained using a Nicolet-6700 FT-IR spectrometer (Thermo Scientific, Madison, WI, USA). Fluorescence spectra were recorded using an F97-Pro fluorospectrophotometer (Lengguang Tech. Ltd., Shanghai, China). UV-Vis absorption spectra were recorded using a UV-vis spectrophotometer (Mapada Instruments Ltd., Shanghai, China). Fluorescence lifetime spectra were measured using F-7000 equipment. The redox properties of DN-CDs were examined by cyclic voltammetry which was carried out on a CH1660A electrochemical workstation.

2.5. Detection of Metal Ions

The PL spectra were measured to study the selectivity and sensitivity of the DN-CDs. The different chemical compounds with different metal ions (Na⁺, K⁺, Ca²⁺, Fe²⁺, Fe³⁺, Cr³⁺, Mg²⁺, Mn²⁺, Pb²⁺, Zn²⁺, Cd²⁺) and anions (SO₄²⁻, PO₄³⁻, Cl⁻, NO₃⁻) were dissolved in DI-water to obtain a series of metal solutions with a concentration of 10 μM. 1 mL aqueous solution of metal ions and 1 mL aqueous solution of DN-CDs (20 μg/mL) were mixed. After a certain amount of time, PL intensity was detected three times to obtain the average value. To further study the sensitivity detection of Cu²⁺, a series of CuSO₄ solutions with concentration of 0–500 μM were prepared and mixed with 1 mL DN-CDs (20 μg/mL). A Cu²⁺ solution was added into the solutions containing other metal ions to obtain a mixed solution with two metal ions to conduct interference tests.

2.6. Detection in Real Samples

We used the tap water from our laboratory, the water from Jinjiang River in Wuhou District, Chengdu, and the water from a lotus pond in the Wangjiang Campus of Sichuan University as the real water samples. These samples were filtered through a 0.22 μm membrane and centrifuged at 10,000 rpm for 5 min to remove any suspended materials. Then, 1 mL of the sample with a standard Cu²⁺ ion solution (10, 20 and 30 μM) was mixed with 1 mL of DN-CD solution for 4 min and the fluorescence intensity was measured.

3. Results and Discussion

3.1. Optical Properties of DN-CDs

In this study, by changing the ratio of CA and DETA, reaction temperature and reaction time, we developed a simple one-step synthesis method for carbon dots with a high quantum yield under down-conversion fluorescence. As shown in Figure S1, it could be seen that with the increase in DETA and reaction temperature, the quantum yield first increased and then decreased. Additionally, in Figure 1c, the quantum yield decreased and then increased slightly. Finally, carbon dots with a high quantum yield under down-conversion fluorescence were obtained. Additionally, the optimum conditions were found to be CA/DETA = 1:4, reaction time of 4 h, and reaction temperature of 200 °C. And we used these carbon dots, denoted as DN-CDs, to perform the further characterizations.

The optical properties of the DN-CDs were measured using UV-vis absorption and PL spectroscopy, as shown in Figure 1a. Typically, the absorption of carbon dots could be divided into two main regions: $\pi-\pi^*$ and $n-\pi^*$ transition [52]. The weak absorption peak at 241 nm was the $\pi-\pi^*$ transition of C=C, attributed to the absorption peak of the carbon atom in cyclic aromatic hydrocarbons [53]. The wide absorption peak at 350 nm indicated the $n-\pi^*$ transition of the nitrogen- or oxygen-containing functional groups on the surface of the DN-CDs, attributed to the doping with N atoms [54]. The bandgap energies were determined according to the Tauc plot (Equation (2)) as follows:

$$(ah\nu)^{\frac{1}{n}} = A(h\nu - E_g) \quad (2)$$

where 'a' is the absorption coefficient, 'h' is Planck's constant, 'v' is the incident light frequency, 'E_g' is the bandgap energy, 'A' is a constant and 'v' is a variable dependent on the type of bandgap [55]. As shown in Figure 1b, the bandgap of DN-CDs was 3.21 eV.

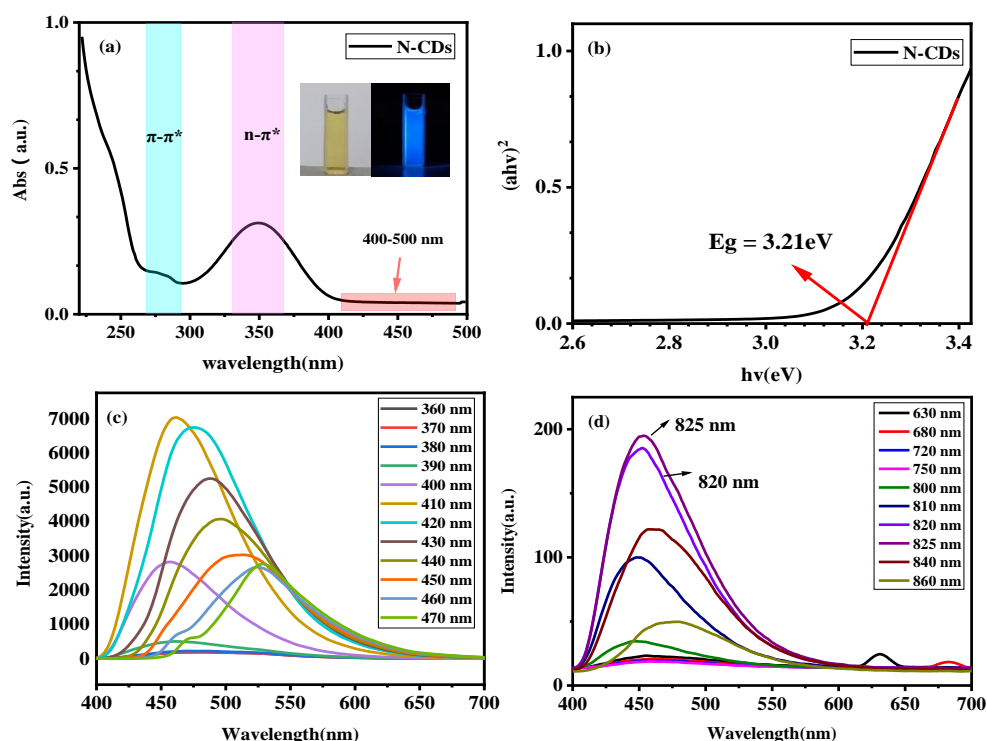


Figure 1. UV-Vis absorption and PL spectra of the DN-CDs. (* represents antibonding molecular orbital) (a) The UV-Vis absorption of DN-CDs. Inset: photograph taken under daylight and 365 nm UV light. (b) The Tauc plot according to the UV-Vis absorption. (The carbon dots are usually indirect bandgaps, so we selected the value of 'n' as 2) (c) Emission spectra of DN-CDs at different excitation wavelengths. (d) Up-conversion emission spectra of DN-CDs at different excitation wavelengths.

Under daylight, the DN-CD solution was slightly yellow and clear; in contrast, it was a bright blue color if exposed to UV irradiation at 365 nm (inset in Figure 1a). Figure 1c displayed the photoluminescence spectra of DN-CDs, showing a maximum emission at 450 nm ($\lambda_{ex} = 410$ nm). Moreover, when the excitation wavelength was increased, the peak value of fluorescence had a small red shift, which indicated that the PL was dependent on the excitation wavelength. This excitation-dependent fluorescence property reflected the size of the DN-CDs and the distribution of different surface states [56]. In particular, Figure 1d also demonstrates the stable up-conversion PL property. When the excitation wavelength changed from 630 nm to 860 nm, the UCPL spectrum showed a basically unchanged emission at 451 nm, indicating a single emission center in the carbon dots. The peak intensities at 820 and 825 nm were significantly higher than that of other wavelengths. The doping with N atoms might lead to an increase in lone pair electrons on oxygen atoms and nitrogen atoms, increasing the electron density in the π -system. Additionally, it would reduce the π^* -energy level of the excitation, so the excitation required a lower energy [35].

3.2. Photoluminescence Stability of DN-CDs

For the application of fluorescent probes in the detection of metal ions, it is important to explore the up-conversion fluorescence (UCPL) stability of DN-CDs. The PL intensity of DN-CDs under different pH conditions is shown in Figure 2a, indicating a strong UCPL intensity in a wide range of pH levels (pH = 4–12). In particular, DN-CDs had a negligible change in the PL emission range or intensity within pH levels of 4–9, indicating excellent stability of the DN-CDs; the UCPL intensity markedly changed under strong acid–base conditions, due to the protonation and deprotonation of the functional groups (-OH/-COOH and -NH₂) on the surface of the DN-CDs, which resulted in the destruction of the aromatic conjugate system and complex system [24,57]. This was proven by the Zeta potentials in different pH aqueous solutions in Figure S2. DN-CDs had a negative potential at pH = 4–13, and the negative potential increased sharply under highly alkaline conditions. DN-CDs had a high positive potential at pH = 2, which indicated that the same protonation in a strong acidic environment. Meanwhile, the DN-CDs had a higher negative potential at pH = 11–13, which indicated intense deprotonation. In order to study the optical stability of carbon dots, we tested their up-conversion fluorescence intensity under daily storage conditions and simulated sunlight conditions using a xenon lamp (300 W). As shown in Figure 2b, we could see that the up-conversion fluorescence intensity of the DN-CD solution remained high after 90 days, which indicated that the DN-CDs had long-time UCPL stability; at the same time, the carbon dot solution was still clear and transparent. As shown in Figure 2c, the up-conversion fluorescence intensity of the carbon dot solution was basically unchanged within the first hour of xenon irradiation (300 W), where F_0 is the initial up-conversion fluorescence intensity, and F is the up-conversion fluorescence intensity after xenon irradiation. In summary, the prepared carbon dots (DN-CDs) had strong pH stability and optical stability.

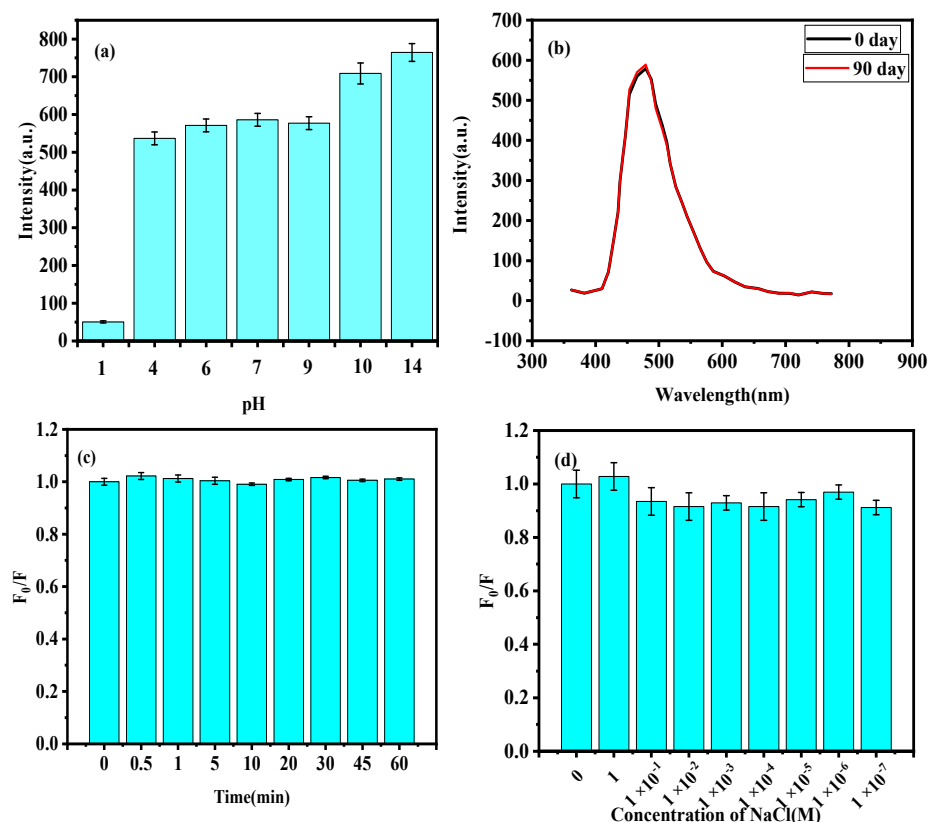


Figure 2. (a) The effect of pH on the UCPL intensity of DN-CDs in a range from 1 to 13. (b) The effect of storage time on PL intensity of DN-CDs after 90 days. (c) The effect of 60 min of UV irradiation on the UCPL intensity (F_0 is the initial UCPL intensity and F is the UCPL intensity after under UV irradiation). (d) The effect of salt concentration on the UCPL intensity for DN-CDs at different concentrations of NaCl (F_0 is the PL intensity of a blank sample and F is the intensity of the experimental sample).

3.3. Morphological and Surface Properties of DN-CDs

The morphological and surface properties of the DN-CDs were investigated by TEM, FT-IR, XRD and XPS; the results are shown in Figures 3 and 4. DN-CDs were nearly spherical with a size distribution between 1.5 and 4.5 nm and the average particle size was about 2.4 nm (Figure 3a,b). Furthermore, the dynamic light scattering (DLS) results in Figure S3 showed that the dynamic diameter of the DN-CDs was about 2.7 nm, which was basically consistent with the TEM. Additionally, we also tested the DLS of DN-CDs in strong acidic and alkaline environments, and found that there was a slight aggregation phenomenon with strong acids, with average size of 3.7 nm. This was also consistent with the fluorescence and Zeta potential changes under strong acidic conditions in Section 3.2. Meanwhile, we found that the crystalline lattice fringe had a space of 0.21 nm, which corresponded to the (100) lattice of graphene in the inset in Figure 3a. Through the Zeta potential of the DN-CDs, it was suggested that the DN-CDs had a negative charge (Figure S3). This was attributed to the partial ionization of the hydroxyl or carboxyl groups in the DN-CDs, which caused the formation of oxygen negative ions. Figure 3c shows the XRD pattern of the DN-CDs with broad peaks at $2\theta = 23.9^\circ$, indicating that the carbon atom in DN-CDs was amorphous. Additionally, this also could be verified in the Raman spectrum of N-CDs in Figure S4. This demonstrated that the fluorescence properties of DN-CDs were mainly determined by the surface groups of the carbon dots.

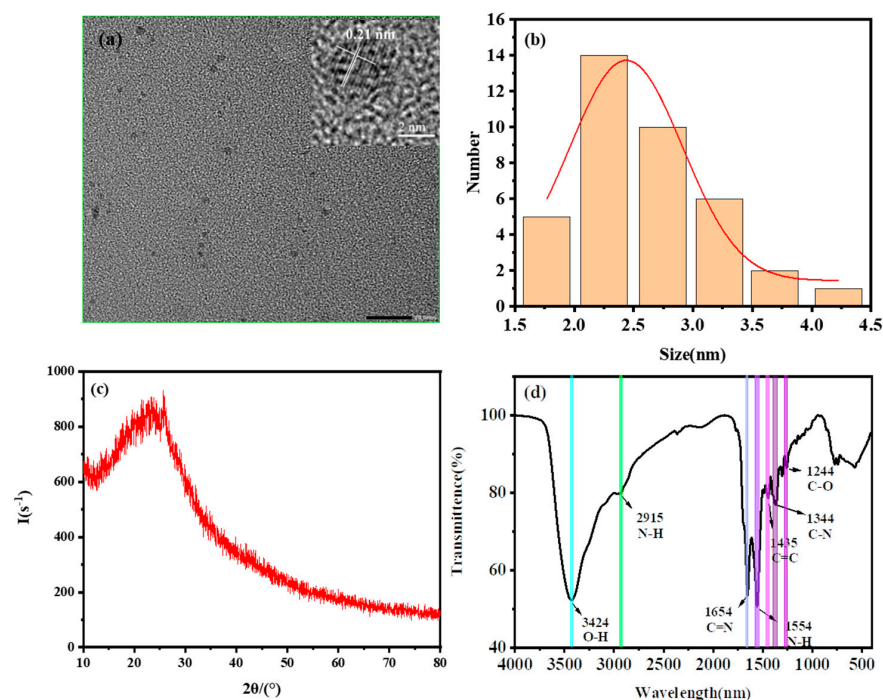


Figure 3. TEM image (a), size distribution (b), XRD spectra (c) and FT-IR spectra (d) of DN-CDs (the inset in (a) is the HRTEM of the DN-CDs).

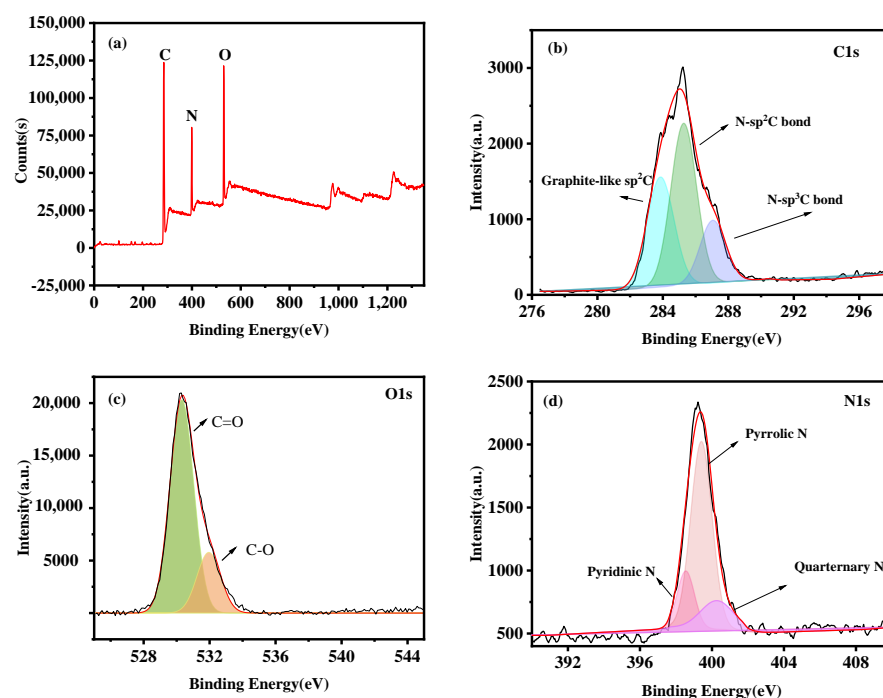


Figure 4. (a) The full-scan XPS spectra of the DN-CDs; (b) C1s spectra of the DN-CDs; (c) O1s spectra of the DN-CDs; (d) N1s spectra of the DN-CDs.

FT-IR spectra were obtained to detect the functional groups of the DN-CDs. As shown in Figure 3d, the DN-CDs exhibited absorption peaks at 3423 cm^{-1} and 2915 cm^{-1} , consistent with -OH and N-H stretch vibrations, showing that the DN-CDs had good water-solubility and contained amino groups on their surfaces. Compared with the FT-IR spectra of DETA, the absorption peak of N-H decreased, indicating that the amine group of DETA and the carboxyl group of citric acid had undergone a dehydration reaction.

In addition, the absorption peaks at 1244 cm^{-1} and 1344 cm^{-1} represented the stretch vibrations of C-O and amide C-N, respectively. The absorption peaks at 1654 cm^{-1} and 1554 cm^{-1} were related to the typical stretch vibrations of C=N and N-H. The absorption peak of 1435 cm^{-1} was the typical stretch vibration of C=C due to the establishment of an unsaturated aromatic ring structure during the hydrothermal treatment. Moreover, it was confirmed by FT-IR spectra that some of the carbonyl groups of citric acid were converted into amide groups in the hydrothermal process. These functional groups improved the hydrophilicity of the DN-CDs in an aqueous system, suggesting the potential of DN-CDs as sensors for aqueous samples.

The elemental composition of the DN-CDs was examined through XPS (Figure 4). As shown in Figure 4a, according to the XPS full-scan profile of the DN-CDs, C, N and O exhibited distinct peaks in the spectra at 284.71 eV, 399.83 eV and 530.95 eV corresponding to the binding energies of C1s, N1s and O1s, respectively. Moreover, the contents of C, N, and O elements in the DN-CDs were 38.4%, 44.1%, and 17.5%, respectively, according to the EDS results (Figure S5). Figure 4b shows three peaks at 284.7 eV, 285.9 eV and 287.5 eV related to the binding energies of graphite-like C_{sp^2} , N- C_{sp^2} and N- C_{sp^3} bonds, respectively. The O1s spectra showed two peaks at 530.38 eV and 532.02 eV, attributed to the binding energy of C=O and C-O, respectively (Figure 4c). Additionally, the N1s spectra showed that it could be deconvoluted into three peaks at 398.8 eV, 400.5 eV and 401.2 eV which were consistent with the binding energies of pyridinic N, pyrrolic N and quarternary N, respectively (Figure 4d). The large amount of pyrrolic N indicated that most of the N atoms existed in a π conjugated system. In summary, we confirmed that the N elements were successfully doped onto the structure of the carbon dots.

3.4. DN-CDs as a Photoluminescent Probe for Cu^{2+} Ions

To investigate the potential use of the DN-CDs as a PL probe, we examined the effects of different metal ions on PL intensity (Figure 5). It could be seen from Figure 5a that at the same concentration, Na^+ , K^+ , Ca^{2+} , Fe^{2+} , Fe^{3+} , Cr^{3+} , Mg^{2+} , Mn^{2+} , Pb^{2+} , Zn^{2+} and Cd^{2+} ions basically did not change the PL intensity of the carbon dots; with the same concentration of Cu^{2+} , the PL intensity was 60% of that of the control, showing an obvious fluorescence quenching phenomenon. In addition, the interference of other metal ions on the detection of Cu^{2+} was examined by adding the mixed solution of various metal ions and Cu^{2+} into the DN-CDs solution. Meanwhile, the effect of the addition of other metal ions on the detection of Cu^{2+} ions could be nearly ignored, which indicated that DN-CDs had excellent selective quenching for Cu^{2+} . Moreover, we also explored the quenching kinetics of the DN-CDs by monitoring the PL intensity as a function of time. Figure 5b showed that the PL intensity of the DN-CD solution gradually weakened and finally stabilized with increasing Cu^{2+} ions concentration. This result indicated that the detection of Cu^{2+} ions in the DN-CD system was a rapid and effective process and the equilibrium was reached within 3 min. Thus, 3 min was chosen as the detection time in the following experiments.

To investigate the sensitivity of the DN-CDs for detecting Cu^{2+} , the PL spectra of the DN-CDs were examined by adding Cu^{2+} solution at various concentrations (2.5–50 μM). Obviously, in Figure 5c, the intensity of PL quenching increased when the concentration of Cu^{2+} increased; therefore, the decrease in PL intensity was caused by the Cu^{2+} ions instead of the associated anions and was quantitatively related to the Cu^{2+} concentration. This indicated that the DN-CDs were capable of quantitatively detecting Cu^{2+} at low levels with high sensitivity. Additionally, the PL quenching spectra of Cu^{2+} was analyzed by the Stern–Volmer (Equation (3)):

$$\frac{F_0}{F} = K_{sv}[Q] + 1 \quad (3)$$

where ' F_0 ' and ' F ' are the PL intensities of the DN-CDs in the absence and presence of Cu^{2+} , respectively, ' Q ' is the concentration of Cu^{2+} and ' K_{sv} ' is the Stern–Volmer quenching constant. This equation could represent the relationship between the relative PL intensity (F_0/F) and Cu^{2+} concentration (Q).

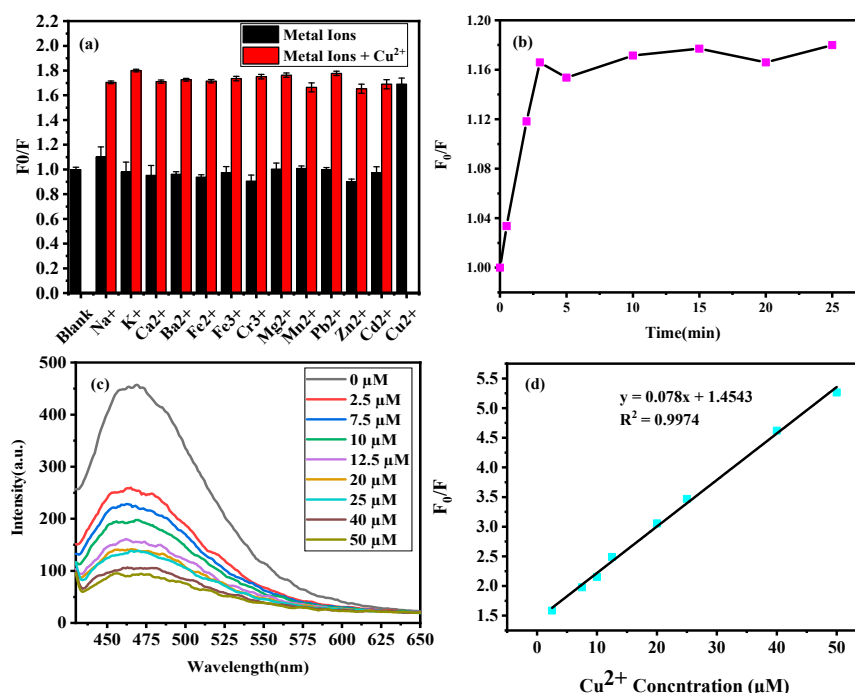


Figure 5. (a) The selectivity of DN-CDs to various metal ions: relative PL intensity of the DN-CDs (20 $\mu\text{g}/\text{mL}$) in the absence (black column) and presence (red column) of other metal ions (10 μM) ($\lambda_{\text{ex}} = 820 \text{ nm}$ and $\lambda_{\text{em}} = 450 \text{ nm}$); (b) the effect of reaction time on the quenching equilibrium of DN-CDs; (c) PL quenching efficiency of DN-CDs at different concentrations of Cu^{2+} ions (2.5–50 μM); (d) the linear relationship between PL intensity and Cu^{2+} ion concentration (F_0 is the PL intensity in the absence of Cu^{2+} ions and F is in the presence of Cu^{2+} ions).

According to Equation (3), we observed strong linearity with a correlation coefficient (R^2) of 0.9974 when the concentration of Cu^{2+} changed from 2.5 to 50 μM . The linear relationship curve is shown in Figure 5d. Based on Equation $\text{LOD} = 3 \cdot \sigma / S$ (where σ is the standard deviation of the blank PL intensity of DN-CDs and S is the slope of the linear relationship curve), the limit of detection (LOD) of Cu^{2+} , was calculated to be 42 nM. Compared with the threshold of the United States Environmental Protection Agency (USEPA) guidelines, the LOD of the DN-CDs for Cu^{2+} in an aqueous system was much lower. We summarized the PL sensing performances of the other reported sensors for detecting Cu^{2+} in Table 1; it was clear that the LOD of our product was also lower than those of the other sensors.

Table 1. The range of detection and LOD of other PL sensors for Cu^{2+} ions.

Sensor	Range of Detection	LOD	Ref.
BP/NS-CDs	0–50 μM	0.18 μM	[24]
OPD-CDs	0.5–40 μM	0.28 μM	[23]
NS-CDs	1–10 μM	0.29 μM	[58]
FA-MoO _x QDs	0.2–500 μM	29 nM	[59]
HBT-H	0–5 μM	0.308 μM	[60]
Fe ₃ O ₄ @SiO ₂ -PAP	0.1–0.2 mg/L	0.125 μM	[61]

3.5. Mechanism of DN-CD Interaction with Cu^{2+}

3.5.1. Exploration of Quenching Mechanism

Carbon dots have already been used in the field of PL sensors and the PL quenching mechanisms of carbon dots had been discussed in other articles. The quenching mechanisms can be roughly divided into two types, which included static quenching and dynamic quenching. There were also other mechanisms, such as Förster resonance energy transfer

(FRET), photo-induced electron transfer (PET) and inner filter effect (IFE). Static quenching would occur through the interaction between the carbon dots and metal ions, forming a non-fluorescent ground-state complex. The existence of the non-fluorescent complex could be verified by UV-Vis spectra. If there was complexation between the functional groups in the carbon dots and metal ions, the absorption peaks on the spectra would have a corresponding blue shift or red shift or even produce an obvious new absorption peak due to a new chemical bond. Dynamic quenching would be caused by the collision of carbon dots through the mechanisms of charge transfer or energy transfer, so that the excited state of the carbon dots would return to its ground state. In contrast to static quenching, dynamic quenching would only affect the excited state of the carbon dots, so there would be no change in the UV-Vis spectra. However, a significant change in the lifetime of fluorescence would be detected. FRET would occur when the emission spectra of the carbon dots overlapped with the absorption spectra of the metal ions due to long range dipole–dipole interactions between the excited state of carbon dots and the ground state of metal ions. Additionally, if a FRET mechanism existed, it could change the lifetime of fluorescence. PET could be defined that the electron transfer would occur between carbon dots (as electron donor or electron receptor) and metal ions (as electron donor or electron receptor), if there is an energy gap between the lowest unoccupied molecular orbitals (LUMO) and the highest occupied molecular orbitals (HOMO) between the carbon dots and metal ions. Additionally, IFE would result from an overlap of the absorption spectra of the metal ions with the excitation or emission spectra of the carbon dots. This could cause energy transfer between the carbon dots and metal ions. Therefore, in this part, we explored the quenching mechanisms of our DN-CDs in detecting Cu^{2+} as static quenching, FRET, PET or IFE by UV-vis spectra.

As shown in Figure 6a, the absorption peak of the DN-CD solution did not change after adding the Cu^{2+} solution compared with the absorption peak without the Cu^{2+} solution, proving that there was no static quenching behavior in our DN-CD PL sensor system.

To explore other possible quenching mechanisms, we compared the PL spectra of DN-CDs with the absorption spectra of the Cu^{2+} aqueous solution (Figure 6b). This indicated that the significant fluorescence emission peak of DN-CDs at 450 nm basically did not overlap with the absorption peak of Cu^{2+} . This concluded that there was no FRET quenching mechanism between the DN-CDs and Cu^{2+} . At the same time, as shown in Figure 6c, there was no obvious overlap between the absorption spectra and fluorescence emission spectra of DN-CDs. Additionally, we used the up-conversion PL as the excitation wavelength, which was far from the absorption wavelength of Cu^{2+} (Figure S6). This could eliminate the IFE effect of the PL quenching progress, which might reduce the number of photons available for the DN-CDs [62].

The fluorescence lifetime decay of DN-CDs in the absence and presence of Cu^{2+} were measured at $\lambda_{\text{ex}} = 820 \text{ nm}$ and $\lambda_{\text{em}} = 450 \text{ nm}$ (Figure 6d). After adding a certain amount of Cu^{2+} solution, the fluorescence lifetime of the DN-CD solution decreased from 10.69 ns to 5.14 ns. This suggested that dynamic quenching occurred in the sensor system. Additionally, we proposed a non-radiative electron-transfer mechanism (PET). We calculated the highest occupied molecular orbital (HOMO) and lowest unoccupied molecular (LUMO) energy levels of the DN-CDs according to the following Equation (4) [63]:

$$E_{\text{LUMO}} = -e(E_{\text{Red}} + 4.4)E_{\text{HOMO}} = -e(E_{\text{Ox}} + 4.4)E_{\text{HOMO}} = E_{\text{LUMO}} - E_{\text{g}} \quad (4)$$

where ' E_{Ox} ' and ' E_{Red} ' are the onset of oxidation and reduction potential of DN-CDs, respectively, and ' E_{g} ' is the optical energy gap resulting from the UV-Vis adsorption. Additionally, the ' E_{Red} ' was -0.69 eV according to the CV plot (Figure S7). The ' E_{LUMO} ' was calculated to be -3.71 eV and ' E_{HOMO} ' was calculated to be -6.92 eV . Obviously, the band gap could overlap the crystal field stabilization energy of Cu^{2+} (1.98 eV) [64]. As illustrated in Figure 7, the excited electrons of the DN-CDs were prone to transfer to the d orbital of Cu^{2+} [65]. Thus, the fluorescence was suppressed and became a partially non-radiative progress.

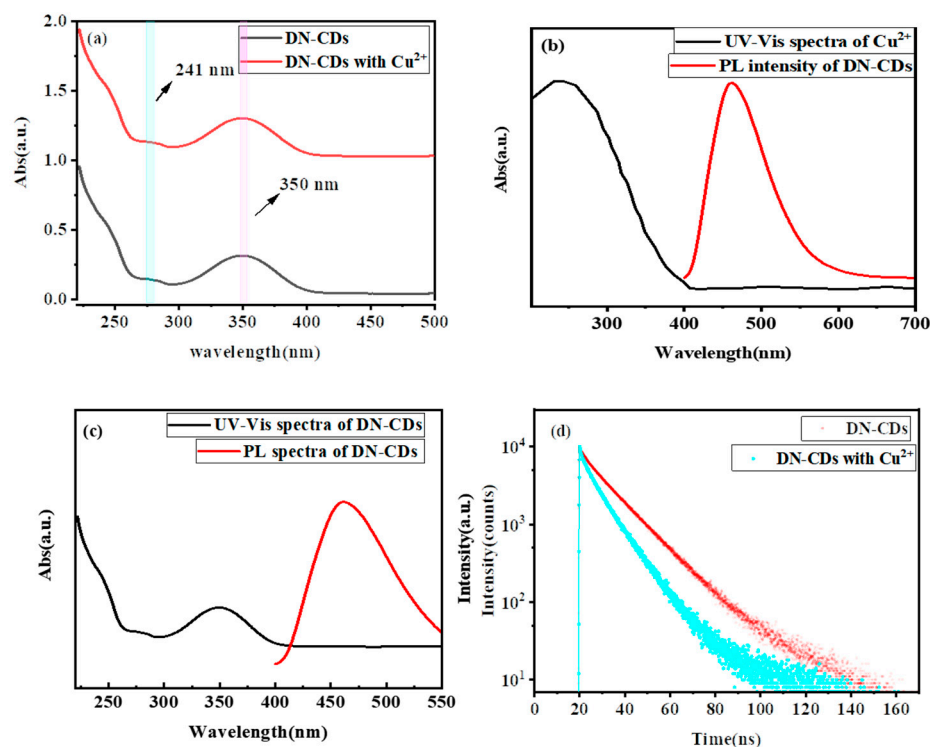


Figure 6. (a) The UV-Vis spectra of DN-CDs in the absence and presence of Cu^{2+} ions; (b) the comparison of the absorption spectra of Cu^{2+} ions and the emission spectra of DN-CDs at $\lambda_{\text{exc}} = 820 \text{ nm}$; (c) the UV-Vis spectra and emission spectra of DN-CDs at $\lambda_{\text{exc}} = 820 \text{ nm}$; (d) the fluorescence lifetime decay of DN-CDs in the absence and presence of Cu^{2+} ions ($\lambda_{\text{exc}} = 410 \text{ nm}$ and $\lambda_{\text{em}} = 450 \text{ nm}$).

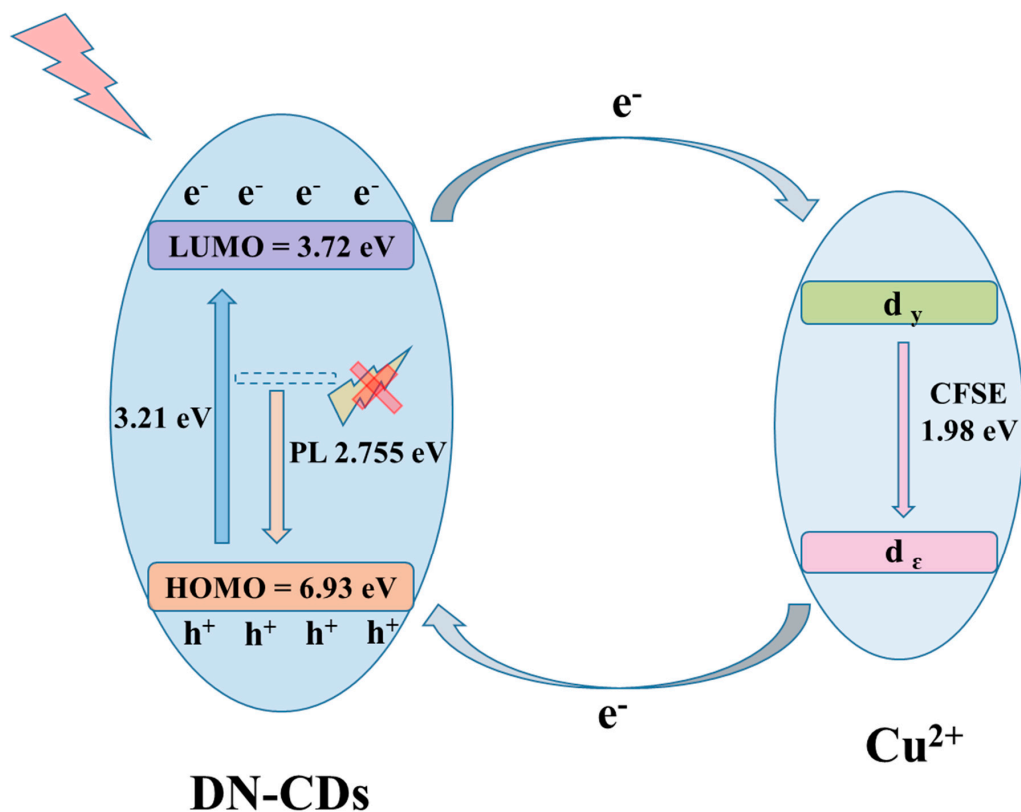


Figure 7. The mechanism of fluorescence quenching detection for Cu^{2+} .

3.5.2. Discussion on the Selectivity of Cu^{2+} and Fe^{3+} Ions

We synthesized two other N-doped carbon dots in our laboratory named N-CDs-1 and N-CDs-2 and we found that they were capable of detecting Fe^{3+} ions. The PL spectra and FT-IR spectra demonstrated that we had successfully synthesized the previously reported carbon dots (Figure S8). The specific and detailed steps of detection of metal ions by these two carbon dots are displayed in the supporting information.

The results of testing the selectivity of N-CDs-1 and N-CDs-2 to metal ions are shown in Figure 8. As seen in Figure 8a, under the same conditions, obvious fluorescence quenching occurred after adding the Fe^{3+} solution to the carbon dot solutions. In contrast, other metal ions had little influence on the PL intensity of N-CDs-1. N-CDs-1 also had an up-conversion PL, so its UCPL sensing system was investigated. The result was consistent with the above one showing that N-CDs-1 with up-conversion PL was also selective for Fe^{3+} ions. Similarly, N-CDs-2 showed selectivity for the detection of Fe^{3+} as shown in Figure 8c. The addition of Fe^{3+} ions caused a strong quenching of the PL intensity, with a quenching degree of more than 80%. Instead, the highest quenching effect of the other ions was only 40% (CrCl_3), which might be due to the larger band gap of the carbon dots, which could overlap with the crystal field energy of Cr^{3+} and produce PET behaviors. In summary, N-CDs-1 and N-CDs-2 could detect Fe^{3+} ions with a good linear relationship in the 1–1000 μM and 20–100 μM ranges and the LODs were 100 nM and 3.93 μM , respectively (Figure S9).

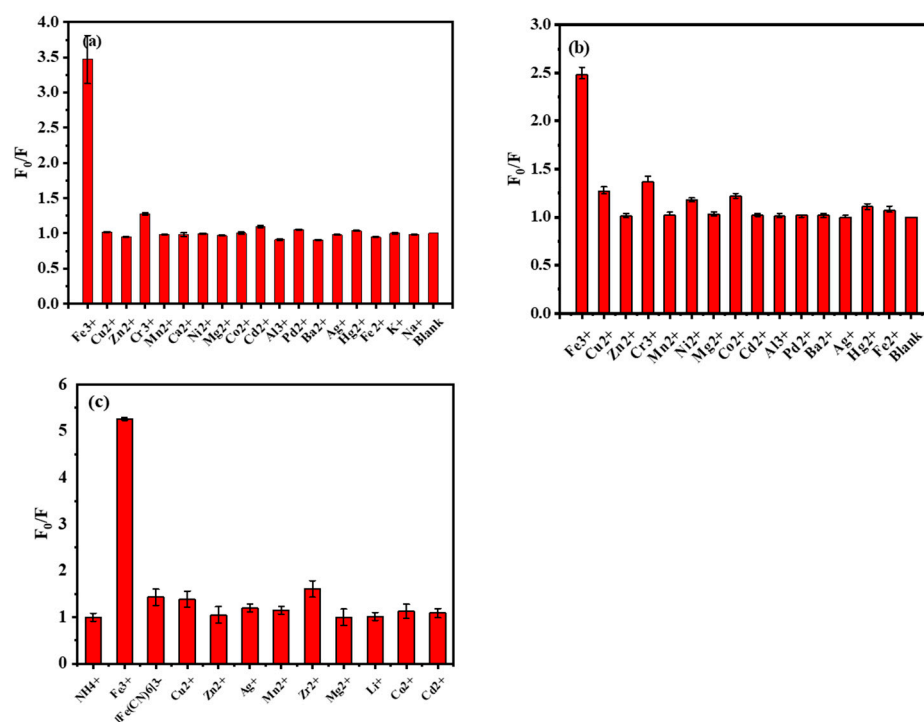


Figure 8. (a) The selectivity of N-CDs-1 to various metal ions at $\lambda_{ex} = 410$ nm, $\lambda_{em} = 510$ nm and (b) $\lambda_{ex} = 808$ nm, $\lambda_{em} = 510$ nm; (c) the selectivity of N-CDs-2 to various metal ions at $\lambda_{ex} = 380$ nm, $\lambda_{em} = 450$ nm.

We were interested in the similarities and differences between the three N-doped carbon dots which could detect Cu^{2+} and Fe^{3+} ions. Through the comparison of the differences between DN-CDs, N-CDs-1 and N-CDs-2, the ratio of N and O atoms were found to be a potential reason for the ability to detecting Cu^{2+} and Fe^{3+} ions. Table S1 summarized the detection parameters for the selective detection of metal ions (Cu^{2+} and Fe^{3+}) with the different N-doped carbon dots [66–79]. It could be found that although N-doped carbon dots contained different electron-rich functional groups, we suggest that the proportion of the N, O atoms might affect the selectivity towards Cu^{2+} and Fe^{3+} ions. The carbon dots with relatively rich N-based groups and more N atoms were more likely

to selectively detect Cu^{2+} ions. More simply, the selective detection of Cu^{2+} and Fe^{3+} ions by carbon dots could be adjusted or converted by altering the ratio of N and O atoms. Moreover, the ratio of N/O of DN-CDs, N-CDs-1 and N-CDs-2 were 14.8:15.6, 21.7:12.8 and 27.1:5.2, which are consistent with our conclusion.

Hence, we preliminarily concluded that the selective detection of Cu^{2+} or Fe^{3+} ions by N-doped carbon dots could be estimated according to the ratio of N/O: when the ratio of N/O is about 1:1 or higher, the N-doped carbon dots tend to selectively detect Cu^{2+} ions; when the N/O ratio is about 1:2 or smaller, the N-doped carbon dots prefer to selectively detect Fe^{3+} ions. The Hard-Soft-Acid-Base theory could explain the difference: 'acids' and 'bases' can be classified as 'hard' or 'soft'. 'Hard' refers to particles with a higher charge density and smaller radius, while 'soft' refers to particles with a lower charge density and larger radius. The interactions between a soft acid and soft base are more stable, while the interactions between a hard acid and hard base are more stable. Thus, Cu^{2+} ions are a borderline acid and can more easily interact with N atoms with a lower electronegativity and bigger radius; Fe^{3+} ions are similar to hard acids, so they are more likely to interact with O atoms with a higher electronegativity and smaller radius. Of course, the quenching mechanisms of carbon dots are complex and other situations would also exist, which require more detailed analysis methods.

3.6. Detection of Cu^{2+} Ions in Real Samples

To prove the practical application of the synthesized DN-CDs, we investigated the ability of the DN-CDs to detect Cu^{2+} ions in water samples as shown in Table S2. The relative standard deviations (RSDs) of Cu^{2+} ion detection in the three samples were less than 8% and the recovery rates were in the range of 95.4–105.9%. This verified that the DN-CDs have great potential in Cu^{2+} ion detection.

4. Conclusions

In conclusion, N-doped carbon dots with down-conversion and up-conversion fluorescence were synthesized by a simple one-step hydrothermal method. The prepared carbon dots, DN-CDs, had excellent fluorescence properties, good stability and a high quantum yield QY of 63.87%. They showed a significant fluorescence intensity at 410 nm, and also had up-conversion fluorescence at 820 nm. Additionally, the abundant N, O-based functional groups endowed the DN-CDs with excellent water solubility and excellent sensitivity and selectivity for Cu^{2+} ion detection with a rapid reaction time of 3 min. Therefore, it had better practicality. We also synthesized other N-doped carbon dots with different carbon sources and nitrogen sources to study their ability to detect metal ions. They had the ability to detect Fe^{3+} ions with a detection limit (LOD) of 100 nM and 3.39 μm . Additionally, although the principle of selective metal ion detection is very complex, by comparing the results in this paper and published reports, a method of synthesizing N-doped carbon dots to detect Cu^{2+} or Fe^{3+} ions exclusively through adjusting the ratio of N and O atoms was proposed: (1) when the ratio of N/O was about 1:1 or higher, the N-doped carbon dots tended to selectively detect Cu^{2+} ions; (2) when the N/O ratio was about 1:2 or smaller, the N-doped carbon dots preferred to selectively detect Fe^{3+} ions. This provided a possible direction for the design and synthesis of N-doped carbon dots with the ability to detect Cu^{2+} or Fe^{3+} ions in the future.

Supplementary Materials: The following supporting information can be downloaded at: <https://www.mdpi.com/article/10.3390/cryst13050812/s1>, Figure S1: The trends of the quantum yield fluorescence of N-doped carbon dots at different ratio of carbon source and nitrogen source (a), reaction temperature (b), reaction time (c); Figure S2: The Zeta potential of DN-CDs under different pH; Figure S3: The DLS of DN-CDs in aqueous solution at (a) pH = 1, (b) pH = 7 and (c) pH = 13; Figure S4: The Raman spectrum of DN-CDs; Figure S5: The EDS of DN-CDs; Figure S6: The up-conversion PL spectra of DN-CDs. (The emission spectrum at maximum excitation wavelength at 820 nm and the excitation spectrum at the maximum emission wavelength of 450 nm); Figure S7: The CV plot of DN-CDs; Figure S8: (a-c) The fluorescence emission spectra at $\lambda_{\text{exc}} = 450$ nm and

$\lambda_{\text{exc}} = 600$ nm and FT-IR spectra of N-CDs-1; (d-e) The fluorescence emission spectra at $\lambda_{\text{exc}} = 380$ nm and FT-IR spectra of N-CDs-2; Figure S9: The PL quenching efficiency of (a) N-CDs-2 at $\lambda_{\text{exc}} = 380$ nm and (c) N-CDs-1 at $\lambda_{\text{exc}} = 410$ nm and (e) at $\lambda_{\text{exc}} = 808$ nm at different concentration of Fe^{3+} ions and the linear relationship between PL intensity and Fe^{3+} ions ('F0' is PL intensity in the absence of Fe^{3+} ions and 'F' is in the presence of Fe^{3+} ions) of (b) N-CDs-2 at $\lambda_{\text{exc}} = 380$ nm, (d) N-CDs-1 at $\lambda_{\text{exc}} = 410$ nm and (f) at $\lambda_{\text{exc}} = 808$ nm; Table S1: The detection parameters for selective detection of metal ions (Cu^{2+} and Fe^{3+}) with different N-doped carbon dots; Table S2: The detection of Cu^{2+} in real samples.

Author Contributions: Conceptualization, Y.X. and Q.Z.; validation, J.H.; investigation, H.M., P.L. and W.Z.; data curation, M.C., Z.M. and Y.D.; writing—original draft preparation, Y.X.; writing—review and editing, Q.Z.; funding acquisition, Q.Z. All authors have read and agreed to the published version of the manuscript.

Funding: This research was funded by an Industry-university-research cooperation of Sichuan University (No. 19H0340).

Data Availability Statement: The authors confirm that the data supporting the reported results can be found within the article. Other relevant information can be obtained from the author.

Conflicts of Interest: The authors declare that they have no known competing financial interests or personal relationships that could have influenced the work reported in this paper.

References

1. Zhang, R.; Liu, B.; Ma, J.; Zhu, R. Preparation and characterization of carboxymethyl cellulose/chitosan/alginate hydrogels with adjustable pore structure for adsorption of heavy metal ions. *Eur. Polym. J.* **2022**, *179*, 111577. [[CrossRef](#)]
2. Ansari, S.; Karimi, M. Novel developments and trends of analytical methods for drug analysis in biological and environmental samples by molecularly imprinted polymers. *Trends Anal. Chem.* **2017**, *89*, 146–162. [[CrossRef](#)]
3. El-Shahawi, M.S.; Hamza, A.; Bashammakh, A.S.; Al-Saggaf, W.T. An overview on the accumulation, distribution, transformations, toxicity and analytical methods for the monitoring of persistent organic pollutants. *Talanta* **2010**, *80*, 1587–1597. [[CrossRef](#)] [[PubMed](#)]
4. Martín-Pozo, L.; de Alarcón-Gómez, B.; Rodríguez-Gómez, R.; García-Córcoles, M.T.; Çipa, M.; Zafra-Gómez, A. Analytical methods for the determination of emerging contaminants in sewage sludge samples. A review. *Talanta* **2019**, *192*, 508–533. [[CrossRef](#)] [[PubMed](#)]
5. Kumbhar, H.S.; Gadilohar, B.L.; Shankarling, G.S. A highly selective quinaldine–indole based spiropyran with intramolecular H-bonding for visual detection of Cu(II) ions. *Sens. Actuators B Chem.* **2016**, *222*, 35–42. [[CrossRef](#)]
6. Gao, F.; Tu, X.; Yu, Y.; Gao, Y.; Zou, J.; Liu, S.; Qu, F.; Li, M.; Lu, L. Core-shell Cu@C@ZIF-8 composite: A high-performance electrode material for electrochemical sensing of nitrite with high selectivity and sensitivity. *Nanotechnology* **2022**, *33*, 225501. [[CrossRef](#)] [[PubMed](#)]
7. Chen, H.; Yang, T.; Liu, F.; Li, W. Electrodeposition of gold nanoparticles on Cu-based metal-organic framework for the electrochemical detection of nitrite. *Sens. Actuators B Chem.* **2019**, *286*, 401–407. [[CrossRef](#)]
8. Carolan, D.; Doyle, H. Germanium nanocrystals as luminescent probes for rapid, sensitive and label-free detection of Fe^{3+} ions. *Nanoscale* **2015**, *7*, 5488–5494. [[CrossRef](#)]
9. Ferreira, S.L.C.; Bezerra, M.A.; Santos, A.S.; dos Santos, W.N.L.; Novaes, C.G.; de Oliveira, O.M.C.; Oliveira, M.L.; Garcia, R.L. Atomic absorption spectrometry—A multi element technique. *Trends Anal. Chem.* **2018**, *100*, 1–6. [[CrossRef](#)]
10. Matusch, A.; Depboylu, C.; Palm, C.; Wu, B.; Höglinger, G.U.; Schäfer, M.K.H.; Becker, J.S. Cerebral bioimaging of Cu, Fe, Zn, and Mn in the MPTP mouse model of Parkinson's disease using laser ablation inductively coupled plasma mass spectrometry (LA-ICP-MS). *J. Am. Soc. Mass. Spectrom.* **2010**, *21*, 161–171. [[CrossRef](#)]
11. Trung, L.G.; Subedi, S.; Dahal, B.; Truong, P.L.; Gwag, J.S.; Tran, N.T.; Nguyen, M.K. Highly efficient fluorescent probes from chitosan-based amino-functional carbon dots for the selective detection of Cu^{2+} traces. *Mater. Chem. Phys.* **2022**, *291*, 126772. [[CrossRef](#)]
12. Xu, H.; Zhou, S.; Xiao, L.; Wang, H.; Li, S.; Yuan, Q. Fabrication of a nitrogen-doped graphene quantum dot from MOF-derived porous carbon and its application for highly selective fluorescence detection of Fe^{3+} . *J. Mater. Chem. C* **2015**, *3*, 291–297. [[CrossRef](#)]
13. Yang, C.-X.; Ren, H.-B.; Yan, X.-P. Fluorescent Metal–Organic Framework MIL-53(Al) for Highly Selective and Sensitive Detection of Fe^{3+} in Aqueous Solution. *Anal. Chem.* **2013**, *85*, 7441–7446. [[CrossRef](#)]
14. Mohandoss, S.; Palanisamy, S.; You, S.; Lee, Y.R. Synthesis of cyclodextrin functionalized photoluminescent metal nanoclusters for chemoselective Fe^{3+} ion detection in aqueous medium and its applications of paper sensors and cell imaging. *J. Mol. Liq.* **2022**, *356*, 118999. [[CrossRef](#)]

15. Xin, J.-Y.; Li, Y.; Liu, F.-Y.; Sun, L.-R.; Wang, Y.; Xia, C.-G. Visible and Ultraviolet Dual-Readout Detection of Cu(II) in Preserved Vegetables Based on Self-Assembly and Peroxidase Simulation Properties of Mb-AuNPs. *Sci. Adv. Mater.* **2022**, *14*, 1410–1418. [[CrossRef](#)]
16. Cetinkaya, Y.; Yurt, M.N.Z.; Avni Oktem, H.; Yilmaz, M.D. A Monostyryl Boradiazaindacene (BODIPY)-based lanthanide-free colorimetric and fluorogenic probe for sequential sensing of copper (II) ions and dipicolinic acid as a biomarker of bacterial endospores. *J. Hazard. Mater.* **2019**, *377*, 299–304. [[CrossRef](#)]
17. Zhu, S.; Meng, Q.; Wang, L.; Zhang, J.; Song, Y.; Jin, H.; Zhang, K.; Sun, H.; Wang, H.; Yang, B. Highly photoluminescent carbon dots for multicolor patterning, sensors, and bioimaging. *Angew. Chem. Int. Ed. Engl.* **2013**, *52*, 3953–3957. [[CrossRef](#)]
18. Han, Z.; Nan, D.; Yang, H.; Sun, Q.; Pan, S.; Liu, H.; Hu, X. Carbon quantum dots based ratiometric fluorescence probe for sensitive and selective detection of Cu²⁺ and glutathione. *Sens. Actuators B Chem.* **2019**, *298*, 126842. [[CrossRef](#)]
19. Mitra, S.; Chakraborty, A.J.; Tareq, A.M.; Emran, T.B.; Nainu, F.; Khuroo, A.; Idris, A.M.; Khandaker, M.U.; Osman, H.; Alhumaydhi, F.A.; et al. Impact of heavy metals on the environment and human health: Novel therapeutic insights to counter the toxicity. *J. King. Saud. Univ. Sci.* **2022**, *34*, 101865. [[CrossRef](#)]
20. Zhou, W.; Mo, F.; Sun, Z.; Luo, J.; Fan, J.; Zhu, H.; Zhu, Z.; Huang, J.; Zhang, X. Bright red-emitting P, Br co-doped carbon dots as “OFF-ON” fluorescent probe for Cu²⁺ and L-cysteine detection. *J. Alloys Compd.* **2022**, *897*, 162731. [[CrossRef](#)]
21. Kumari, A.; Kumar, A.; Sahu, S.K.; Kumar, S. Synthesis of green fluorescent carbon quantum dots using waste polyolefins residue for Cu²⁺ ion sensing and live cell imaging. *Sens. Actuators B Chem.* **2018**, *254*, 197–205. [[CrossRef](#)]
22. Li, H.; Xu, T.; Zhang, Z.; Chen, J.; She, M.; Ji, Y.; Zheng, B.; Yang, Z.; Zhang, S.; Li, J. Photostable and printable fluorescence carbon quantum dots for advanced message encryption and specific reversible multiple sensing of Cu²⁺ and cysteine. *Chem. Eng. J.* **2023**, *453*, 139722. [[CrossRef](#)]
23. Lv, W.; Lin, M.; Li, R.; Zhang, Q.; Liu, H.; Wang, J.; Huang, C. Aggregation-induced emission enhancement of yellow photoluminescent carbon dots for highly selective detection of environmental and intracellular copper(II) ions. *Chin. Chem. Lett.* **2019**, *30*, 1410–1414. [[CrossRef](#)]
24. Sonaimuthu, M.; Ganesan, S.; Anand, S.; Kumar, A.J.; Palanisamy, S.; You, S.; Velsankar, K.; Sudhakar, S.; Lo, H.-M.; Lee, Y.R. Multiple heteroatom dopant carbon dots as a novel photoluminescent probe for the sensitive detection of Cu²⁺ and Fe³⁺ ions in living cells and environmental sample analysis. *Environ. Res.* **2023**, *219*, 115106. [[CrossRef](#)]
25. Jiang, D.; Zheng, M.; Yan, X.; Huang, B.; Huang, H.; Gong, T.; Liu, K.; Liu, J. A “turn-on” ESIPT fluorescence probe of 2-(aminocarbonyl)phenylboronic acid for the selective detection of Cu(ii). *RSC Adv.* **2022**, *12*, 31186–31191. [[CrossRef](#)] [[PubMed](#)]
26. Mahajan, P.G.; Dige, N.C.; Vanjare, B.D.; Eo, S.-H.; Kim, S.J.; Lee, K.H. A nano sensor for sensitive and selective detection of Cu²⁺ based on fluorescein: Cell imaging and drinking water analysis. *Spectrochim. Acta A* **2019**, *216*, 105–116. [[CrossRef](#)]
27. Issa, M.A.; Abidin, Z.Z.; Sobri, S.; Rashid, S.A.; Mahdi, M.A.; Ibrahim, N.A. Fluorescent recognition of Fe³⁺ in acidic environment by enhanced-quantum yield N-doped carbon dots: Optimization of variables using central composite design. *Sci. Rep.* **2020**, *10*, 11710. [[CrossRef](#)] [[PubMed](#)]
28. Nagaraj, M.; Ramalingam, S.; Murugan, C.; Aldawood, S.; Jin, J.-O.; Choi, I.; Kim, M. Detection of Fe³⁺ ions in aqueous environment using fluorescent carbon quantum dots synthesized from endospore of *Borassus flabellifer*. *Environ. Res.* **2022**, *212*, 113273. [[CrossRef](#)]
29. Wang, Y.; Chang, Q.; Hu, S. Carbon dots with concentration-tunable multicolored photoluminescence for simultaneous detection of Fe³⁺ and Cu²⁺ ions. *Sens. Actuators B Chem.* **2017**, *253*, 928–933. [[CrossRef](#)]
30. Yuan, Y.H.; Liu, Z.X.; Li, R.S.; Zou, H.Y.; Lin, M.; Liu, H.; Huang, C.Z. Synthesis of nitrogen-doping carbon dots with different photoluminescence properties by controlling the surface states. *Nanoscale* **2016**, *8*, 6770–6776. [[CrossRef](#)]
31. Zhang, H.; Chen, Y.; Liang, M.; Xu, L.; Qi, S.; Chen, H.; Chen, X. Solid-phase synthesis of highly fluorescent nitrogen-doped carbon dots for sensitive and selective probing ferric ions in living cells. *Anal. Chem.* **2014**, *86*, 9846–9852. [[CrossRef](#)]
32. Mejía Ávila, J.; Rangel Ayala, M.; Kumar, Y.; Pérez-Tijerina, E.; Robles, M.A.R.; Agarwal, V. Avocado seeds derived carbon dots for highly sensitive Cu (II)/Cr (VI) detection and copper (II) removal via flocculation. *Chem. Eng. J.* **2022**, *446*, 137171. [[CrossRef](#)]
33. Rahmani, Z.; Ghaemy, M. One-step hydrothermal-assisted synthesis of highly fluorescent N-doped carbon dots from gum tragacanth: Luminescent stability and sensitive probe for Au³⁺ ions. *Opt. Mater.* **2019**, *97*, 109356. [[CrossRef](#)]
34. Luo, T.; Bu, L.; Peng, S.; Zhang, Y.; Zhou, Z.; Li, G.; Huang, J. One-step microwave-assisted preparation of oxygen-rich multifunctional carbon quantum dots and their application for Cu²⁺-curcumin detection. *Talanta* **2019**, *205*, 120117. [[CrossRef](#)] [[PubMed](#)]
35. Zhao, Q.; Li, X.; Wang, X.; Zang, Z.; Liu, H.; Li, L.; Yu, X.; Yang, X.; Lu, Z.; Zhang, X. Surface amino group modulation of carbon dots with blue, green and red emission as Cu²⁺ ion reversible detector. *Appl. Surf. Sci.* **2022**, *598*, 153892. [[CrossRef](#)]
36. Xu, J.; Wang, C.; Li, H.; Zhao, W. Synthesis of green-emitting carbon quantum dots with double carbon sources and their application as a fluorescent probe for selective detection of Cu²⁺ ions. *RSC Adv.* **2020**, *10*, 2536–2544. [[CrossRef](#)]
37. Jiao, T.; Wen, H.; Dong, W.; Wen, W.; Li, Z. Metal ion (Fe³⁺ and Cu²⁺) catalyzed synthesis of high quantum yield carbon dots. *Mater. Lett.* **2022**, *324*, 132575. [[CrossRef](#)]
38. Siahcheshm, P.; Heiden, P. High quantum yield carbon quantum dots as selective fluorescent turn-off probes for dual detection of Fe²⁺/Fe³⁺ ions. *J. Photochem. Photobiol. A* **2023**, *435*, 114284. [[CrossRef](#)]
39. Atabaev, T.S. Doped carbon dots for sensing and bioimaging applications: A minireview. *Nanomaterials* **2018**, *8*, 342. [[CrossRef](#)]

40. Gao, X.; Du, C.; Zhuang, Z.; Chen, W. Carbon quantum dot-based nanoprobe for metal ion detection. *J. Mater. Chem. C* **2016**, *4*, 6927–6945. [[CrossRef](#)]
41. Molaei, M.J. Principles, mechanisms, and application of carbon quantum dots in sensors: A review. *Anal. Methods* **2020**, *12*, 1266–1287. [[CrossRef](#)]
42. Mohandoss, S.; Ganesan, S.; Palanisamy, S.; You, S.; Velsankar, K.; Sudhakar, S.; Lo, H.-M.; Lee, Y.R. Nitrogen, sulfur, and phosphorus Co-doped carbon dots-based ratiometric chemosensor for highly selective sequential detection of Al³⁺ and Fe³⁺ ions in logic gate, cell imaging, and real sample analysis. *Chemosphere* **2023**, *313*, 137444. [[CrossRef](#)] [[PubMed](#)]
43. Tian, L.; Li, Z.; Wang, P.; Zhai, X.; Wang, X.; Li, T. Carbon quantum dots for advanced electrocatalysis. *J. Energy Chem.* **2021**, *55*, 279–294. [[CrossRef](#)]
44. Salehtabar, F.; Ghaemy, M. Preparation of strongly photoluminescent nanocomposite from DGEBA epoxy resin and highly fluorescent nitrogen-doped carbon dots. *Polym. Bull.* **2023**, *80*, 3247–3264. [[CrossRef](#)]
45. Liu, R.; Haruna, S.A.; Ali, S.; Xu, J.; Ouyang, Q.; Li, H.; Chen, Q. An Up-conversion signal probe-MnO₂ nanosheet sensor for rapid and sensitive detection of tetracycline in food. *Spectrochim. Acta A* **2022**, *270*, 120855. [[CrossRef](#)]
46. Fu, A.C.; Hu, Y.; Zhao, Z.-H.; Su, R.; Song, Y.; Zhu, D. Functionalized paper microzone plate for colorimetry and up-conversion fluorescence dual-mode detection of telomerase based on elongation and capturing amplification. *Sens. Actuators B Chem.* **2018**, *259*, 642–649. [[CrossRef](#)]
47. Liang, J.-M.; Zhang, F.; Zhu, Y.-L.; Deng, X.-Y.; Chen, X.-P.; Zhou, Q.-J.; Tan, K.-J. One-pot hydrothermal synthesis of Si-doped carbon quantum dots with up-conversion fluorescence as fluorescent probes for dual-readout detection of berberine hydrochloride. *Spectrochim. Acta A* **2022**, *275*, 121139. [[CrossRef](#)]
48. Fu, J.; Zhou, S.; Tang, S.; Wu, X.; Zhao, P.; Tang, K.; Chen, Y.; Yang, Z.; Zhang, Z. Imparting down/up-conversion dual channels fluorescence to luminescence metal-organic frameworks by carbon dots-induced for fluorescence sensing. *Talanta* **2022**, *242*, 123283. [[CrossRef](#)]
49. Deng, Y.; Chen, M.; Chen, G.; Zou, W.; Zhao, Y.; Zhang, H.; Zhao, Q. Visible–Ultraviolet Upconversion Carbon Quantum Dots for Enhancement of the Photocatalytic Activity of Titanium Dioxide. *ACS Omega* **2021**, *6*, 4247–4254. [[CrossRef](#)]
50. Mao, Z.; Li, H.; Gan, N.; Suo, Z.; Zhang, H.; Zhao, Q. Contribution of nicotinamide as an intracyclic N dopant to the structure and properties of carbon dots synthesized using three α -hydroxy acids as C sources. *Nanotechnology* **2022**, *33*, 215705. [[CrossRef](#)]
51. Fang, C.; Lihua, Z.; Hong, W. Preparation of Carbon Dots and Determination of Their Fluorescence Quantum Yield. *Univ. Chem.* **2019**, *34*, 67–72.
52. Ali, M.; Anjum, A.S.; Bibi, A.; Wageh, S.; Sun, K.C.; Jeong, S.H. Gradient heating-induced bi-phase synthesis of carbon quantum dots (CQDs) on graphene-coated carbon cloth for efficient photoelectrocatalysis. *Carbon* **2022**, *196*, 649–662. [[CrossRef](#)]
53. Liang, C.; Xie, X.; Shi, Q.; Feng, J.; Zhang, D.; Huang, X. Nitrogen/sulfur-doped dual-emission carbon dots with tunable fluorescence for ratiometric sensing of ferric ions and cell membrane imaging. *Appl. Surf. Sci.* **2022**, *572*, 151447. [[CrossRef](#)]
54. Chen, X.; Song, Z.; Yuan, B.; Li, X.; Li, S.; Thang Nguyen, T.; Guo, M.; Guo, Z. Fluorescent carbon dots crosslinked cellulose Nanofibril/Chitosan interpenetrating hydrogel system for sensitive detection and efficient adsorption of Cu (II) and Cr (VI). *Chem. Eng. J.* **2022**, *430*, 133154. [[CrossRef](#)]
55. Preeyanghaa, M.; Vinesh, V.; Sabarikirishwaran, P.; Rajkamal, A.; Ashokkumar, M.; Neppolian, B. Investigating the role of ultrasound in improving the photocatalytic ability of CQD decorated boron-doped g-C₃N₄ for tetracycline degradation and first-principles study of nitrogen-vacancy formation. *Carbon* **2022**, *192*, 405–417. [[CrossRef](#)]
56. Dong, Y.; Pang, H.; Yang, H.B.; Guo, C.; Shao, J.; Chi, Y.; Li, C.M.; Yu, T. Carbon-Based Dots Co-doped with Nitrogen and Sulfur for High Quantum Yield and Excitation-Independent Emission. *Angew. Chem. Int. Ed.* **2013**, *52*, 7800–7804. [[CrossRef](#)]
57. Gao, Y.; Zhang, H.; Jiao, Y.; Lu, W.; Liu, Y.; Han, H.; Gong, X.; Shuang, S.; Dong, C. Strategy for Activating Room-Temperature Phosphorescence of Carbon Dots in Aqueous Environments. *Chem. Mater.* **2019**, *31*, 7979–7986. [[CrossRef](#)]
58. Wang, H.; Wang, P.; Niu, L.; Liu, C.; Xiao, Y.; Tang, Y.; Chen, Y. Carbazole-thiophene based fluorescent probe for selective detection of Cu²⁺ and its live cell imaging. *Spectrochim. Acta A* **2022**, *278*, 121257. [[CrossRef](#)]
59. Kateshiya, M.R.; Malek, N.I.; Kailasa, S.K. Folic acid functionalized molybdenum oxide quantum dots for the detection of Cu²⁺ ion and alkaline phosphatase via fluorescence turn off–on mechanism. *Spectrochim. Acta A* **2022**, *268*, 120659. [[CrossRef](#)]
60. Zhao, L.-X.; Chen, K.-Y.; Xie, K.-B.; Hu, J.-J.; Deng, M.-Y.; Zou, Y.-L.; Gao, S.; Fu, Y.; Ye, F. A benzothiazole-based “on-off” fluorescence probe for the specific detection of Cu²⁺ and its application in solution and living cells. *Dye. Pigm.* **2023**, *210*, 110943. [[CrossRef](#)]
61. Zhang, Y.; Zhu, T.; Xu, Y.; Yang, Y.; Sheng, D.; Ma, Q. Quaternized salicylaldehyde Schiff base side-chain polymer-grafted magnetic Fe₃O₄ nanoparticles for the removal and detection of Cu²⁺ ions in water. *Appl. Surf. Sci.* **2023**, *611*, 155632. [[CrossRef](#)]
62. John, B.K.; John, N.; Korah, B.K.; Thara, C.; Abraham, T.; Mathew, B. Nitrogen-doped carbon quantum dots as a highly selective fluorescent and electrochemical sensor for tetracycline. *J. Photochem. Photobiol. A* **2022**, *432*, 114060. [[CrossRef](#)]
63. Sun, S.; Bao, W.; Yang, F.; Yan, X.; Sun, Y.; Zhang, G.; Yang, W.; Li, Y. Electrochemical synthesis of Fe_Nx doped carbon quantum dots for sensitive detection of Cu²⁺ ion. *Green. Energy Environ.* **2021**, *8*, 141–150. [[CrossRef](#)]
64. Bossu, F.P.; Chellappa, K.L.; Margerum, D.W. Ligand effects on the thermodynamic stabilization of copper(III)-peptide complexes. *J. Am. Chem. Soc.* **1977**, *99*, 2195–2203. [[CrossRef](#)] [[PubMed](#)]

65. Wang, J.; Sheng Li, R.; Zhi Zhang, H.; Wang, N.; Zhang, Z.; Huang, C.Z. Highly fluorescent carbon dots as selective and visual probes for sensing copper ions in living cells via an electron transfer process. *Biosens. Bioelectron.* **2017**, *97*, 157–163. [[CrossRef](#)] [[PubMed](#)]
66. Wu, H.; Pang, L.-F.; Fu, M.-J.; Guo, X.-F.; Wang, H. Boron and nitrogen co-doped carbon dots as fluorescence sensor for Fe³⁺ with improved selectivity. *J. Pharm. Biomed. Anal.* **2020**, *180*, 113052. [[CrossRef](#)]
67. Zhang, Z.; Chen, X.; Wang, J. Bright blue emissions N-doped carbon dots from a single precursor and their application in the trace detection of Fe³⁺ and F⁻. *Inorg. Chim. Acta* **2021**, *515*, 120087. [[CrossRef](#)]
68. Zhou, Y.; Chen, G.; Ma, C.; Gu, J.; Yang, T.; Li, L.; Gao, H.; Xiong, Y.; Wu, Y.; Zhu, C.; et al. Nitrogen-doped carbon dots with bright fluorescence for highly sensitive detection of Fe³⁺ in environmental waters. *Spectrochim. Acta A Mol. Biomol. Spectrosc.* **2023**, *293*, 122414. [[CrossRef](#)]
69. Zhang, W.J.; Liu, S.G.; Han, L.; Luo, H.Q.; Li, N.B. A ratiometric fluorescent and colorimetric dual-signal sensing platform based on N-doped carbon dots for selective and sensitive detection of copper (II) and pyrophosphate ion. *Sens. Actuators B Chem.* **2019**, *283*, 215–221. [[CrossRef](#)]
70. Yang, L.; Zeng, J.; Quan, T.; Liu, S.; Deng, L.; Kang, X.; Xia, Z.; Gao, D. Liquid-liquid extraction and purification of oil red O derived nitrogen-doped highly photoluminescent carbon dots and their application as multi-functional sensing platform for Cu²⁺ and tetracycline antibiotics. *Microchem. J.* **2021**, *168*, 106391. [[CrossRef](#)]
71. Yang, F.; Zhou, P.; Duan, C. Solid-phase synthesis of red dual-emissive nitrogen-doped carbon dots for the detection of Cu²⁺ and glutathione. *Microchem. J.* **2021**, *169*, 106534. [[CrossRef](#)]
72. Pranerad, J.; Thongsai, N.; Supchocksoonthorn, P.; Kladsomboon, S.; Paoprasert, P. Multipurpose sensing applications of biocompatible radish-derived carbon dots as Cu²⁺ and acetic acid vapor sensors. *Spectrochim. Acta A* **2019**, *211*, 59–70. [[CrossRef](#)] [[PubMed](#)]
73. Li, Z.; Zhou, Q.; Li, S.; Liu, M.; Li, Y.; Chen, C. Carbon dots fabricated by solid-phase carbonization using p-toluidine and l-cysteine for sensitive detection of copper. *Chemosphere* **2022**, *308*, 136298. [[CrossRef](#)]
74. Krishnaiah, P.; Atchudan, R.; Perumal, S.; Salama, E.-S.; Lee, Y.R.; Jeon, B.-H. Utilization of waste biomass of *Poa pratensis* for green synthesis of n-doped carbon dots and its application in detection of Mn²⁺ and Fe³⁺. *Chemosphere* **2022**, *286*, 131764. [[CrossRef](#)]
75. Gao, B.; Chen, D.; Gu, B.; Wang, T.; Wang, Z.; Xie, F.; Yang, Y.; Guo, Q.; Wang, G. Facile and highly effective synthesis of nitrogen-doped graphene quantum dots as a fluorescent sensing probe for Cu²⁺ detection. *Curr. Appl. Phys.* **2020**, *20*, 538–544. [[CrossRef](#)]
76. Liu, L.; Qin, K.; Yin, S.; Zheng, X.; Li, H.; Yan, H.; Song, P.; Ji, X.; Zhang, Q.; Wei, Y.; et al. Bifunctional carbon dots derived from an anaerobic bacterium of *porphyromonas gingivalis* for selective detection of Fe and bioimaging. *Photochem. Photobiol.* **2021**, *97*, 574–581. [[CrossRef](#)]
77. Fu, Y.; Zhao, S.; Wu, S.; Huang, L.; Xu, T.; Xing, X.; Lan, M.; Song, X. A carbon dots-based fluorescent probe for turn-on sensing of ampicillin. *Dye. Pigment.* **2020**, *172*, 107846. [[CrossRef](#)]
78. Qian, Z.; Shan, X.; Chai, L.; Ma, J.; Chen, J.; Feng, H. Si-doped carbon quantum dots: A facile and general preparation strategy, bioimaging application, and multifunctional sensor. *ACS Appl. Mater. Interfaces* **2014**, *6*, 6797–6805. [[CrossRef](#)] [[PubMed](#)]
79. Zhang, L.C.; Yang, Y.M.; Liang, L.; Jiang, Y.J.; Li, C.M.; Li, Y.F.; Zhan, L.; Zou, H.Y.; Huang, C.Z. Lighting up of carbon dots for copper (II) detection using an aggregation-induced enhanced strategy. *Analyst* **2022**, *147*, 417–422. [[CrossRef](#)]

Disclaimer/Publisher’s Note: The statements, opinions and data contained in all publications are solely those of the individual author(s) and contributor(s) and not of MDPI and/or the editor(s). MDPI and/or the editor(s) disclaim responsibility for any injury to people or property resulting from any ideas, methods, instructions or products referred to in the content.